

# Outage Probability Analysis for OTFS in Lossy Communications

Xin Zhang\*, Wensheng Lin\*, Lixin Li\*, Fucheng Yang<sup>†</sup>, Zhu Han<sup>‡</sup> and Tad Matsumoto<sup>§</sup>

\* School of Electronics and Information, Northwestern Polytechnical University, Xi'an, China

<sup>†</sup> Research Institute of Information Fusion, Naval Aviation University, Yantai, China

<sup>‡</sup> University of Houston, Houston, USA

<sup>§</sup>IMT-Atlantic, France, and University of Oulu, Finland, Emeritus.

Email: zxx\_@mail.nwpu.edu.cn; {linwest, lilixin}@nwpu.edu.cn; fucheng85@sina.com;

zhan2@uh.edu; tadeshi.matsumoto@oulu.fi

**Abstract**—This paper analyzes the outage probability of orthogonal time frequency space (OTFS) modulation under a lossy communication scenario. First of all, we introduce the channel model and the vector form representation of OTFS this paper uses. Then, we derive an exact expression of the OTFS outage probability in lossy communication scenarios, using Shannon's lossy source-channel separation theorem. Because the channel is time-varying, calculating the exact outage probability is computationally expensive. Therefore, this paper aims to derive a lower bound of the outage probability, which can relatively easily be calculated. Thus, given the distortion requirement and number of the resolvable paths, we can obtain a performance limit under the optimal condition as a reference. Finally, the experimental results of outage probability are obtained by Monte-Carlo method, and compared with the theoretical results calculated by the closed-form expression of the lower bound.

**Index Terms**—OTFS modulation, outage probability, lossy communications, rate-distortion, lower bound.

## I. INTRODUCTION

Research towards developing sixth-generation (6G) wireless communication networks is currently an emerging hot research topic globally, due to its huge potential in supporting various applications, such as extended reality [1] and massive ultra-low latency communications [2]. Compared to fifth-generation (5G) performance metrics, one of the challenges that 6G will face to is to satisfy the diverse and high-quality communication requirements in high user-terminal mobility scenarios, such as high-speed railways, unmanned aerial vehicles, and low earth orbit satellites [3]. In fact, high-mobility broad band signal transmission over wireless channels imposes challenges that need to overcome frequency selectivity and time selectivity in the presence of fading variations. They are caused by excessive bandwidth and Doppler spread, compared to the channel coherence bandwidth and time, respectively.

Orthogonal frequency division multiplexing (OFDM), which is widely used in 5G and its unprecedented systems, is a

This paper has been accepted for publication in IEEE Globecom 2024 workshop.

This work was supported in part by National Natural Science Foundation of China under Grants 62001387 and 62101450, in part by Young Elite Scientists Sponsorship Program by China Association for Science and Technology under Grant 2022QNRC001, in part by Aeronautical Science Foundation of China under Grants 2022Z021053001 and 2023Z071053007, in part by Shanghai Academy of Spaceflight Technology under Grant SAST2022-052, in part by French National Research Agency Future Program under reference ANR-10-LABX-07-01, in part by NSF CNS-2107216, CNS-2128368, CMMI-2222810, ECCS-2302469, US Department of Transportation, Toyota and Amazon.

robust technique against fading frequency selectivity, however its transmission performance is severely degraded due to the Doppler shift that destroys the orthogonality between subcarriers. In order to eliminate the detrimental effects caused by the doubly dispersive channels, a new modulation technique referred to as orthogonal time frequency space (OTFS) modulation, with which the equivalent channel is defined in the delay-Doppler (DD) domain, is proposed in [4]. It has been widely recognized as a promising approach to reliable and robust communications in high user-terminal mobility scenarios [5]. Different from OFDM, OTFS processes the information symbols in the DD domain, thus transforms the channels suffering from the double selectivity in the time-frequency (TF) domain into quasistatic channels in the DD domain exhibiting sparse and hence separable properties. Therefore, OTFS requires only a lower channel estimation overhead than OFDM. It is worth noting that modulating information symbols are defined in the DD domain, instead of TF domain, and hence each symbol in an OTFS frame experiences the effect of the full fluctuations in the TF channel. Therefore, OTFS has the potential to exploit the full channel diversity, yielding better error performance in the high user-terminal mobility scenarios.

It is worth mentioning the representative researches aiming at realizing the practical OTFS system. DD channel response needs to be estimated for OTFS signal detection at the receiver. In [6], pilot-aided channel estimation techniques are studied. Furthermore, detection algorithms have also been proposed for OTFS signal detection. Raviteja *et al.* [7] proposes a low-complexity detector based on message passing (MP) algorithm. They estimate inter-symbol interference component as a Gaussian variable to reduce the detection complexity.

Notice that current OTFS researches almost focus on lossless communications. However, a big tendency of wireless communication concept creation is a joint design with artificial intelligence (AI) [8]–[11], where the recovered information should not necessarily be lossless. As long as the final decision made by AI is correct, lossy recovery at the decoder output still can be effectively exploited [12], [13]. Therefore, lossy communications have a great potential for AI-oriented communications in 6G. Even though the previous contributions mentioned above have provided stringent framework for practical OTFS system designs, the outage probability of OTFS has not been thoroughly analyzed, especially for lossy

communications.

Due to the random channel variation in the DD domain, the instantaneous channel capacity may not always support lossless transmission of the information sequence, in which case the information recovered at the receiver may well be lossy. Notice that it is challenging to derive the explicit expression of distortion under the instantaneous channel capacity constraints. We can utilize equivalent source coding based on Shannon's lossy source-channel separation theorem to equivalently determine the distortion corresponding to the channel capacity [14]. Hence, determining the outage performance of OTFS in lossy communications is of significant importance.

Given the background described above, we are motivated to investigate the outage probability of OTFS in lossy communications. The main contributions of this paper include: 1) Employing an equivalent source coding method based on Shannon's lossy source-channel separation theorem for determining the signal-to-noise ratio (SNR) corresponding to the distortion requirement with the aim of calculating the outage probability; 2) Deriving the exact expression for the outage probability with OTFS in lossy communications, given the distortion on requirement and resolvable path number; 3) Deriving the lower bound of the outage probability without requiring heavy computational complexity.

## II. SYSTEM MODEL

This section provides a general description of the DD domain channel model and the vector form representation of the OTFS channel in the DD domain, and then introduces the achievable capacity with the considered system model.

### A. Channel Model

The received signal  $r(t)$  transmitted from a transmitter with an input signal  $s(t)$  over the DD domain channel is given by

$$r(t) = \iint h(\tau, \nu) s(t - \tau) e^{j2\pi\nu(t - \tau)} d\nu d\tau + w(t). \quad (1)$$

Assume that  $w(t)$  is an additive white Gaussian noise (AWGN) with one-sided power spectral density (PSD)  $N_0$ . Only a few parameters are often needed to model the channel in the DD domain, since there are typically only a small number of reflectors in the channel with associated delays and Doppler shifts. Due to the sparsity of the channel representation, the response  $h(\tau, \nu)$  is expressed in the following form:

$$h(\tau, \nu) = \sum_{i=1}^P h_i \delta(\tau - \tau_i) \delta(\nu - \nu_i), \quad (2)$$

where  $\delta(\cdot)$  is the Dirac delta function,  $P$  is the number of independent resolvable paths, and  $h_i$ ,  $\tau_i$  and  $\nu_i$  denote, respectively, the complex fading coefficient, delay and Doppler shift corresponding to the  $i$ -th path.

We assume that a cyclic prefix (CP) of length  $L_{CP}$  is appended to the sequence to be sent before transmission. Specifically, we denote the delay and the Doppler indice by  $l_i$  and  $k_i$ , where  $\tau_i = \frac{l_i}{M\Delta f}$  and  $\nu_i = \frac{k_i}{NT}$ . Specifically, with

$0 \leq l_i \leq l_{max}$ ,  $l_{max}$  is usually not greater than  $L_{CP}$ , i.e., the maximum delay of the channel is  $\tau_{max} = l_{max}T/M$ . For the same reason,  $-k_{max} \leq k_i \leq k_{max}$  is assumed, i.e., the maximum Doppler shift is  $\nu_{max} = \frac{k_{max}}{NT}$ . The effect of the fractional delays in typical wide-band systems can be ignored because the sampling period  $\frac{1}{M\Delta f}$  in the delay domain is in common small. Besides, the effects of fractional Doppler shifts from the nearest Doppler grid can be mitigated by adding TF domain windows, when we assume neither receive filter in the Doppler domain nor use sampling frequency higher than the Nyquist sampling rate [15]. Therefore, the results derived in this paper can be straightforwardly extended to the fractional delay and Doppler shifts case.

Let  $\mathbf{h} = [h_1, h_2, \dots, h_P]^T$  denote the channel coefficient vector of size  $P \times 1$ , assuming the elements in  $\mathbf{h}$  are independent and identically distributed (i.i.d.) complex Gaussian random variables. Since the channel coefficients have uniform power delay and Doppler profile,  $h_i$  for  $1 \leq i \leq P$  has mean  $\mu$  and variance  $1/(2P)$  per dimension and does not depend on the delay or Doppler shifts. In particular, with  $\mu = 0$ ,  $|h_i|$  follows the Rayleigh distribution.

### B. Vector Form Representation of OTFS

Let  $M$  represent number of subcarriers and  $N$  number of slots per OTFS frame [4].  $\mathbf{F}_N$  is the normalized discrete Fourier transform matrices of size  $N \times N$ . We then define  $\mathbf{y}$  and  $\mathbf{x}$  to represent the DD domain transmitted and received symbol vectors, respectively.  $\mathbf{w}$  is equivalent sample vector of AWGN in DD domain with one-sided PSD of  $N_0$ . The input-output relationship of OTFS in the DD domain is [16]

$$\mathbf{y} = \mathbf{H}_{DD}\mathbf{x} + \mathbf{w}, \quad (3)$$

where  $\mathbf{H}_{DD}$  is the effective DD domain channel matrix

$$\mathbf{H}_{DD} = \sum_{i=1}^P h_i (\mathbf{F}_N \otimes \mathbf{I}_M) \mathbf{\Pi}^{l_i} \mathbf{\Delta}^{k_i} (\mathbf{F}_N^H \otimes \mathbf{I}_M), \quad (4)$$

with  $\mathbf{\Pi}$  being a forward cyclic shift permutation matrix describing the delay effect, and  $\mathbf{\Delta} = \text{diag}\{\alpha^0, \alpha^1, \dots, \alpha^{MN-1}\}$  being a diagonal matrix describing the Doppler effect with  $\alpha = e^{j\frac{2\pi}{MN}}$  [16].

We now focus on the analysis of the achievable capacity, assuming a two-dimensional (2D) Gaussian codebook with an average symbol energy  $E_s$  for transmission. On the basis of the vector form representation of the input-output relationship in the DD domain, the normalized achievable capacity is calculated as [16]

$$C = I(\mathbf{y}; \mathbf{x}) = \frac{1}{MN} \log_2 \det \left( \mathbf{I}_{MN} + \frac{E_s}{N_0} \mathbf{H}_{DD}^H \mathbf{H}_{DD} \right). \quad (5)$$

Based on the previous analysis of the system model, outage performance analysis is presented in the next section.

## III. OUTAGE PERFORMANCE ANALYSIS

This section gives a definition for the outage probability of OTFS in lossy communications, and then derives the lower bound of the outage probability.

### A. Rate-Distortion Analysis

Assume  $T \times \Delta f = 1$  throughout this paper, i.e., OTFS is critically sampled for all pulse shaping waveforms. For an OTFS system with  $M$  subcarriers and  $N$  time slots, the length of original binary sequence required to be modulated is  $L = M \times N \times K$  per frame, with  $2^K$  being the modulation order. Because the channel variation due to fading is random in time, the instantaneous channel capacity may not be able to support lossless transmission of the original sequence of  $L$  bits. In this case, the information recovered at the receiver is lossy. To equivalently evaluate the distortion of the recovered information sequence, we adopt Shannon's lossy source-channel separation theorem for performance analysis. Based on Shannon's lossy source-channel separation theorem, the original sequence of  $L$  bits is first lossy-compressed into a codeword of length  $S$ ,  $S = M \times N \times R$ , where  $R$  is the target rate. Therefore, the lossy compression rate can be represented as  $R_S = \frac{MNR}{MNR} = \frac{R}{K}$ .

In each OTFS frame, there are  $M$  subcarriers and  $N$  time slots, and hence the corresponding block in the DD domain can be divided into  $M \times N$  resource sub-blocks. Each DD resource sub-block can allocate one symbol to carry information. Assuming that the channel coefficient vector  $\mathbf{h}$  is fixed within one OTFS frame, then the capacity of each DD resource sub-block averaged within one frame can be represented by  $C$  as depicted in Fig. 1. Hence, the information that can be transmitted in one OTFS frame is  $M \times N \times C$ . Thus lossless transmission of the codeword of length  $S$  is guaranteed whenever  $S \leq M \times N \times C$ , i.e.,  $R \leq C$ . Then the receiver can recover a lossy sequence of length  $L$  with distortion  $D$  according to the codeword<sup>1</sup>.

The equivalent system model of OTFS in lossy communications presented in Fig. 1. After inverse symplectic finite Fourier transform (ISFFT) and Heisenberg transform [4], the codeword is transmitted over the channel. Assuming that the signal  $s(t)$  can be transmitted losslessly in the channel. At the receiver, the received signal  $r(t)$  is transformed to the DD domain through the Wigner transform and symplectic finite Fourier transform (SFFT), prior to symbol demodulation. Then, the sequence is restored to its original length  $L$  with distortion  $D$ . According to the rate-distortion theorem, the distortion can be calculated as

$$D = H_b^{-1}(1 - R/K), \quad (6)$$

where  $H_b(\cdot)$  is the binary entropy function. Furthermore, for a binary source, the Hamming distortion is equivalent to the bit error rate (BER), i.e.,  $BER = D$ .

Based on (5) and (6), the outage probability is defined as

$$\begin{aligned} P_{\text{out}} &= \Pr \left\{ \frac{1}{MN} \log_2 \det \left( \mathbf{I}_{MN} + \frac{E_s}{N_0} \mathbf{H}_{\text{DD}}^H \mathbf{H}_{\text{DD}} \right) < R \right\} \\ &= \Pr \left\{ H_b^{-1} \left[ 1 - \frac{1}{MNK} \log_2 \det \left( \mathbf{I}_{MN} + \frac{E_s}{N_0} \mathbf{H}_{\text{DD}}^H \mathbf{H}_{\text{DD}} \right) \right] > D \right\}. \end{aligned} \quad (7)$$

<sup>1</sup>To achieve the performance of Shannon's lossy source-channel separation theorem, the code length has to be long enough. Therefore, the achievable rate-distortion region derived in this paper provides a lower bound.

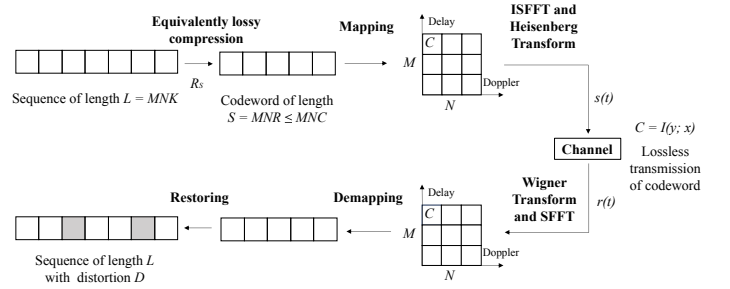


Fig. 1. Equivalent system model of lossy transmissions with OTFS based on lossy source-channel separation theorem.

It is obvious that the outage probability of the OTFS in lossy communications is closely related to the effective DD domain channel matrix  $\mathbf{H}_{\text{DD}}$ . In the next subsection we will investigate the properties of  $\mathbf{H}_{\text{DD}}^H \mathbf{H}_{\text{DD}}$  and derive a lower bound of the outage probability correspondingly.

### B. Lower Bound Derivation

Note that the matrix  $\mathbf{H}_{\text{DD}}^H \mathbf{H}_{\text{DD}}$  is a decomposable Hermitian matrix, i.e., it has nonnegative eigenvalues [16]. Based on (4),  $\mathbf{H}_{\text{DD}}^H \mathbf{H}_{\text{DD}}$  can be written as

$$\begin{aligned} \mathbf{H}_{\text{DD}}^H \mathbf{H}_{\text{DD}} &= \left[ \sum_{i=1}^P h_i^* (\mathbf{F}_N \otimes \mathbf{I}_M) (\Delta^{k_i})^H (\mathbf{\Pi}^{l_i})^H (\mathbf{F}_N^H \otimes \mathbf{I}_M) \right] \\ &\quad \times \left[ \sum_{i=1}^P h_i (\mathbf{F}_N \otimes \mathbf{I}_M) \mathbf{\Pi}^{l_i} \Delta^{k_i} (\mathbf{F}_N^H \otimes \mathbf{I}_M) \right] \\ &= \sum_{i=1}^P |h_i|^2 \mathbf{I}_{MN} + \sum_{i=1}^P \sum_{\substack{i'=1 \\ i' \neq i}}^P h_i^* h_{i'} (\mathbf{F}_N \otimes \mathbf{I}_M) \Delta^{-k_i} \\ &\quad \mathbf{\Pi}^{l_{i'} - l_i} \Delta^{k_{i'}} (\mathbf{F}_N^H \otimes \mathbf{I}_M). \end{aligned} \quad (8)$$

To simplify the expression, we let  $\mathbf{H}_A = \sum_{i=1}^P |h_i|^2 \mathbf{I}_{MN}$  and

$$\begin{aligned} \mathbf{H}_{B1} &= \sum_{i=1}^{P-1} \sum_{\substack{i'=i+1, \\ l_{i'}=l_i}}^P (\mathbf{F}_N \otimes \mathbf{I}_M) (h_i^* h_{i'} \mathbf{\Lambda} + h_i h_{i'}^* \mathbf{\Lambda}^H) (\mathbf{F}_N^H \otimes \mathbf{I}_M), \\ \mathbf{H}_{B2} &= \sum_{i=1}^{P-1} \sum_{\substack{i'=i+1, \\ l_{i'} \neq l_i}}^P (\mathbf{F}_N \otimes \mathbf{I}_M) (h_i^* h_{i'} \mathbf{\Lambda} + h_i h_{i'}^* \mathbf{\Lambda}^H) (\mathbf{F}_N^H \otimes \mathbf{I}_M), \end{aligned} \quad (9)$$

where,  $\mathbf{\Lambda} = \Delta^{-k_i} \mathbf{\Pi}^{l_{i'} - l_i} \Delta^{k_{i'}}$ , hence  $\mathbf{H}_{\text{DD}}^H \mathbf{H}_{\text{DD}} = \mathbf{H}_A + \mathbf{H}_{B1} + \mathbf{H}_{B2}$ . Then, we can obtain the theoretical outage probability of OTFS in lossy communications, as

$$P_{\text{out}} = \iiint_Q dh_{\text{Re},1} dh_{\text{Im},1} \cdots dh_{\text{Re},i} dh_{\text{Im},i}, \quad (10)$$

where,  $Q$  is the region enclosed by

$$H_b^{-1} \left\{ 1 - \frac{1}{MNK} \log_2 \det \left[ \mathbf{I}_{MN} + \frac{E_s}{N_0} (\mathbf{H}_A + \mathbf{H}_{B1} + \mathbf{H}_{B2}) \right] \right\} > D. \quad (11)$$

Notice that it is difficult to obtain a concise closed-form expression of (10). Although  $P_{\text{out}}$  can be calculated using numerical algorithms, its computational complexity is quite

heavy. However, it is found that the calculation of  $P_{out}$  can be simplified by deriving a lower bound, for which we propose two propositions.

*Proposition 1:*

$$\det\left(\mathbf{I}_{MN} + \frac{E_s}{N_0}(\mathbf{H}_A + \mathbf{H}_{B1})\right) \leq \det\left(\mathbf{I}_{MN} + \frac{E_s}{N_0}\mathbf{H}_A\right). \quad (12)$$

The proof of *Proposition 1* is presented in Appendix A.

*Proposition 2:*

$$\det\left(\mathbf{I}_{MN} + \frac{E_s}{N_0}(\mathbf{H}_A + \mathbf{H}_{B1} + \mathbf{H}_{B2})\right) \leq \det\left(\mathbf{I}_{MN} + \frac{E_s}{N_0}(\mathbf{H}_A + \mathbf{H}_{B1})\right). \quad (13)$$

The proof of *Proposition 2* is presented in Appendix B.

Combining *Proposition 1* and *Proposition 2*, we have

$$\det\left(\mathbf{I}_{MN} + \frac{E_s}{N_0}\mathbf{H}_{DD}^H\mathbf{H}_{DD}\right) \leq \det\left(\mathbf{I}_{MN} + \frac{E_s}{N_0}\mathbf{H}_A\right). \quad (14)$$

It matches our intuition that the capacity becomes maximum when the energy from all paths is fully combined without loss. This can give a performance limit under the optimal condition as a reference. Moreover, based on (7), we can deduce the lower bound of  $P_{out}$ :

$$\begin{aligned} P_{out} &\geq \Pr\left\{H_b^{-1}\left[1 - \frac{1}{MNK}\log_2\det\left(\mathbf{I}_{MN} + \frac{E_s}{N_0}\mathbf{H}_A\right)\right] > D\right\} \\ &= \Pr\left\{H_b^{-1}\left[1 - \frac{1}{K}\log_2\left(1 + \frac{E_s}{N_0}\sum_{i=1}^P|h_i|^2\right)\right] > D\right\} \\ &= \Pr\left\{\sum_{i=1}^P|h_i|^2 < \frac{2^{K-KH_b(D)} - 1}{E_s/N_0}\right\}. \end{aligned} \quad (15)$$

To simplify the derivation, we define vector  $\mathbf{h}' = [h'_1, h'_2, \dots, h'_P]^T$  with  $P$  elements, where  $h'_i = \sqrt{2P}h_i$ . As discussed in Section II-A,  $h_i$  follows for any  $i$  an i.i.d complex Gaussian distribution, and hence  $h'_i$  for  $1 \leq i \leq P$  are i.i.d. complex Gaussian random variables with zero mean and unit variance per dimension. Therefore,  $\sum_{i=1}^P|h'_i|^2$  follows a Chi-squared distribution with  $2P$  degrees of freedom. In this way, (15) can be further written as

$$P_{out} \geq \Pr\left\{\sum_{i=1}^P|h'_i|^2 < \frac{2P(2^{K-KH_b(D)} - 1)}{E_s/N_0}\right\}. \quad (16)$$

Eventually, from the probability density function (PDF) of the Chi-square distribution [17, Section 5.8], we can calculate

$$P_{out} \geq 1 - \exp\left(-\frac{P(2^{K-KH_b(D)} - 1)}{E_s/N_0}\right) \sum_{i=0}^{P-1} \frac{P^i(2^{K-KH_b(D)} - 1)^i}{i!(E_s/N_0)^i}. \quad (17)$$

#### IV. PERFORMANCE EVALUATION

In this section, we employed the Monte-Carlo method [18, Section 2.3] to obtain the outage probability experimentally where randomly generated  $h_i$  is used to evaluate the theoretical outage expressed by the multi-fold integral given by (10). They were then compared to the lower-bound outage probability derived in the previous session. Without loss of generality, we set  $\Delta f = 15\text{KHz}$  and  $f_c = 4\text{GHz}$ , and use maximum-ratio combining (MRC) at the detector. The channel

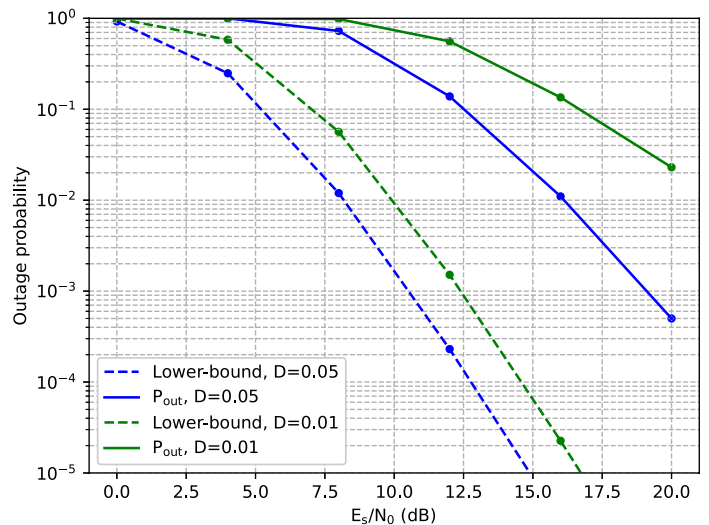


Fig. 2. The outage probability with  $M = N = 16$ ,  $P = 5$ .

coefficients are randomly generated based on the uniform power delay and Doppler profile, as discussed in Section II-A. To facilitate comparison of the results, we fixed  $l_i$  and  $k_i$  in the ranges  $[0, 8]$  and  $[-8, 8]$ , respectively. Therefore, the effect of moving speed on the experimental results can be neglected.

We first demonstrate the lower-bound outage probability and the experimental outage probability for different frame lengths. Fig. 2 illustrates the curves of the lower bound and the experimental of the outage probability versus  $E_s/N_0$  for  $M = N = 16$  and  $P = 5$ . It is clearly seen that the outage probability decreases with greater distortion  $D$ , with the same  $E_s/N_0$ .

Fig. 3 shows the lower bound and the experimental outage probability with  $M = N = 32$ . In high  $E_s/N_0$  value range, the experimental outage probability curve in Fig. 3 has a significantly steeper slope than that in Fig. 2, and is also closer to the lower bound curve. This is because the rate-distortion theorem requires the code length needs to be infinite, so the longer the frame length the smaller the gap. Thus, the longer the frame length, the closer the outage probability is to the actual value. It is also worth noting that in the high  $E_s/N_0$  region, the slope of the experimental outage probability and the corresponding lower bound are essentially the same.

Fig. 4 illustrates the theoretical curves of the OTFS outage probability for different resolvable paths and frame lengths. It is clear that as number of resolvable paths increases, the outage probability decreases under the same conditions. In addition, the outage probability for various frame lengths coincides each other over a relatively large value range of  $E_s/N_0$ . However, the outage probability at  $M = N = 32$  is slightly lower than that at  $M = N = 16$ . The difference of the outage probability becomes larger as  $E_s/N_0$  increases.

#### V. CONCLUSION

We have analyzed the outage probability of OTFS in lossy communications. We start from the rate-distortion analysis of OTFS in lossy communications based on Shannon's lossy

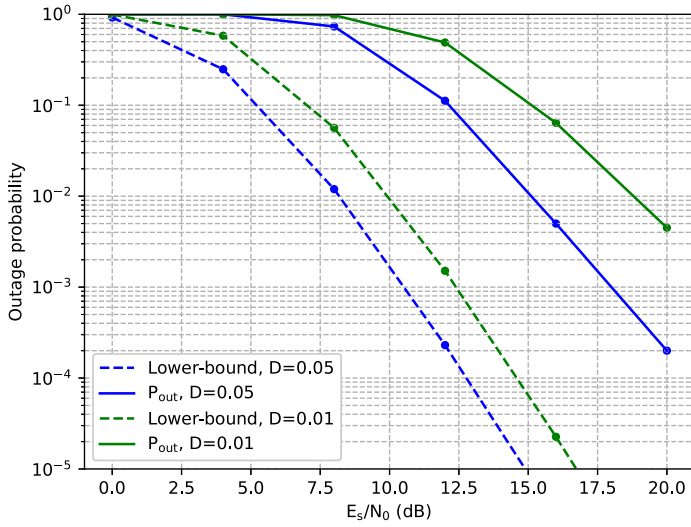


Fig. 3. The outage probability with  $M = N = 32$ ,  $P = 5$ .

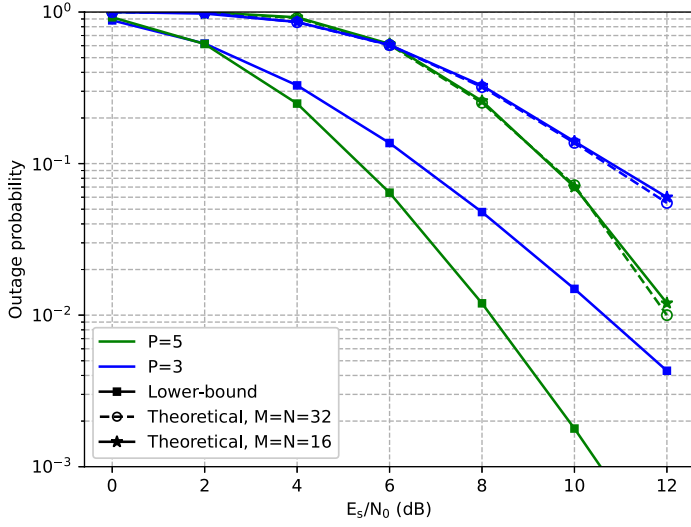


Fig. 4. The outage probability of OTFS in lossy communications with different numbers of paths and frame lengths, where the distortion  $D = 0.05$ .

source-channel separation theorem. Then, we derived an exact expression for the outage probability, expressed by a multi-fold integral with respect to the PDFs of the instantaneous channel coefficients, and hence numerical calculation for the multi-fold integral requires heavy computational complexity. To simplify the calculations, we obtained a lower bound on the outage probability. It has been found that the numerical results are consistent in their curve tendency to the lower bound analysis, and the longer the frame length, the closer the actual outage probability obtained by the Monte-Carlo integral.

#### APPENDIX A PROOF OF Proposition 1

Consider

$$\mathbf{H}_{B1} = \sum_{i=1}^{P-1} \sum_{\substack{i'=i+1, \\ l_{i'}=l_i}}^P (\mathbf{F}_N \otimes \mathbf{I}_M) (h_i^* h_{i'} \mathbf{\Lambda} + h_i h_{i'}^* \mathbf{\Lambda}) (\mathbf{F}_N^H \otimes \mathbf{I}_M)$$

$$= \sum_{i=1}^{P-1} \sum_{\substack{i'=i+1, \\ l_{i'}=l_i}}^P (\mathbf{F}_N \otimes \mathbf{I}_M) \left( h_i^* h_{i'} \Delta^{k_{i'}-k_i} + h_i h_{i'}^* \Delta^{k_i-k_{i'}} \right) (\mathbf{F}_N^H \otimes \mathbf{I}_M), \quad (18)$$

where,  $\mathbf{\Lambda} = \Delta^{-k_i} \mathbf{\Pi}^{l_{i'}-l_i} \Delta^{k_{i'}}$ , when  $l_{i'} = l_i$ ,  $\mathbf{\Lambda} = \Delta^{k_i-k_{i'}}$ . For the ease of derivation, let  $k_{i',i} = k_{i'} - k_i \neq 0$  and  $h_i^* h_{i'} = |h_{i,i'}| e^{j\theta_{i,i'}}$ . Then, we further analyze  $\mathbf{\Theta} = h_i^* h_{i'} \Delta^{k_{i'}-k_i} + h_i h_{i'}^* \Delta^{k_i-k_{i'}}$ , as

$$\begin{aligned} \mathbf{\Theta} &= |h_{i,i'}| e^{j\theta_{i,i'}} \text{diag} \left\{ e^{j\frac{2\pi \times 0}{MN} k_{i',i}}, \dots, e^{j\frac{2\pi(MN-1)}{MN} k_{i',i}} \right\} \\ &\quad + |h_{i,i'}| e^{-j\theta_{i,i'}} \text{diag} \left\{ e^{-j\frac{2\pi \times 0}{MN} k_{i',i}}, \dots, e^{-j\frac{2\pi(MN-1)}{MN} k_{i',i}} \right\} \\ &= |h_{i,i'}| \text{diag} \left\{ e^{j\left(\frac{2\pi \times 0}{MN} k_{i',i} + \theta_{i,i'}\right)} + e^{-j\left(\frac{2\pi \times 0}{MN} k_{i',i} + \theta_{i,i'}\right)}, \dots, \right. \\ &\quad \left. e^{j\left(\frac{2\pi(MN-1)}{MN} k_{i',i} + \theta_{i,i'}\right)} + e^{-j\left(\frac{2\pi(MN-1)}{MN} k_{i',i} + \theta_{i,i'}\right)} \right\} \\ &= 2|h_{i,i'}| \text{diag} \left\{ \cos\left(\frac{2\pi \times 0}{MN} k_{i',i} + \theta_{i,i'}\right), \dots, \right. \\ &\quad \left. \cos\left(\frac{2\pi(MN-1)}{MN} k_{i',i} + \theta_{i,i'}\right) \right\} \\ &= 2|h_{i,i'}| \text{diag} \{\beta_0, \dots, \beta_{MN-1}\}, \quad (19) \end{aligned}$$

where,  $\beta_b = \cos\left(\frac{2\pi b}{MN} k_{i',i} + \theta_{i,i'}\right)$ .

For the convenience of the fast Fourier transform (FFT),  $M$  and  $N$  are integer powers of 2 in most systems. Assume  $k_{i',i} = a_1 \times a_2$ , where,  $a_1$  is odd,  $a_2 = 2^q$ ,  $q \in \{0, 1, \dots, \log_2 N - 1\}$ . Since  $k_{i',i} < N$ ,  $N/a_2$  is integer power of 2 as well. We have

$$\begin{aligned} \beta_{b+\frac{MN}{2a_2}} &= \cos\left(\frac{2\pi\left(b+\frac{MN}{2a_2}\right)}{MN} k_{i',i} + \theta_{i,i'}\right) \\ &= \cos\left(\frac{2\pi b}{MN} k_{i',i} + \pi a_1 + \theta_{i,i'}\right) \\ &= -\cos\left(\frac{2\pi b}{MN} k_{i',i} + \theta_{i,i'}\right) = -\beta_b. \quad (20) \end{aligned}$$

Therefore,  $\text{diag}\{\beta_0, \dots, \beta_{MN-1}\}$  can be divided into  $2a_2$  groups, and the odd group and the next even group have the same value and opposite signs, as

$$\begin{aligned} &\text{diag}\left\{ \underbrace{\beta_0, \dots, \beta_{\frac{MN}{2a_2}-1}}_{\text{1st group}}, \underbrace{\beta_{\frac{MN}{2a_2}}, \dots, \beta_{\frac{2MN}{2a_2}-1}}_{\text{2nd group}}, \dots, \right. \\ &\quad \left. \underbrace{\beta_{\frac{(2a_2-1)MN}{2a_2}}, \dots, \beta_{MN-1}}_{\text{2a}_2\text{-th group}} \right\} \\ &= \text{diag}\left\{ \underbrace{\beta_0, \dots, \beta_{\frac{MN}{2a_2}-1}}_{\text{1st group}}, \underbrace{-\beta_0, \dots, -\beta_{\frac{MN}{2a_2}-1}}_{\text{2nd group}}, \dots, \right\}, \quad (21) \end{aligned}$$

i.e., half of the numbers in  $\text{diag}\{\beta_0, \dots, \beta_{MN-1}\}$  are opposite the other half.

Combining (18) and (19), we have

$$\mathbf{I}_{MN} + \frac{E_s}{N_0} (\mathbf{H}_A + \mathbf{H}_{B1}) = (\mathbf{F}_N \otimes \mathbf{I}_M) \mathbf{\Xi} (\mathbf{F}_N^H \otimes \mathbf{I}_M), \quad (22)$$

where

$$\mathbf{\Xi} = \xi_1 \mathbf{I}_{MN} + \text{diag}\{\xi_{2,0}, \dots, \xi_{2,MN-1}\}, \quad (23)$$

$$\xi_1 = 1 + \frac{E_s}{N_0} \sum_{i=1}^P |h_i|^2, \quad (24)$$

$$\xi_{2,b} = \sum_{i=1}^{P-1} \sum_{\substack{i'=i+1, \\ l_{i'}=l_i}}^P \frac{2E_s}{N_0} |h_{i,i'}| \beta_b. \quad (25)$$

Since  $\Xi$  is a diagonal matrix,

$$\begin{aligned} \det \left( \mathbf{I}_{MN} + \frac{E_s}{N_0} (\mathbf{H}_A + \mathbf{H}_{B1}) \right) &= \det(\Xi) \quad (26) \\ &= \prod_{b=0}^{MN-1} (\xi_1 + \xi_{2,b}). \quad (27) \end{aligned}$$

Because  $\beta_{b+\frac{MN}{2a_2}} = -\beta_b$ , the product of the  $b$ -th and the  $(b + \frac{MN}{2a_2})$ -th terms in (27) becomes

$$\begin{aligned} (\xi_1 + \xi_{2,b}) \left( \xi_1 + \xi_{2,b+\frac{MN}{2a_2}} \right) &= (\xi_1 + \xi_{2,b}) (\xi_1 - \xi_{2,b}) \\ &= \xi_1^2 - \xi_{2,b}^2 \leq \xi_1^2, \quad (28) \end{aligned}$$

Therefore,

$$\det \left( \mathbf{I}_{MN} + \frac{E_s}{N_0} (\mathbf{H}_A + \mathbf{H}_{B1}) \right) \leq \xi_1^{MN} = \det \left( \mathbf{I}_{MN} + \frac{E_s}{N_0} \mathbf{H}_A \right). \quad (29)$$

This finishes the proof of *Proposition 1*.

#### APPENDIX B PROOF OF *Proposition 2*

Consider

$$\begin{aligned} &\det \left( \mathbf{I}_{MN} + \frac{E_s}{N_0} (\mathbf{H}_A + \mathbf{H}_{B1} + \mathbf{H}_{B2}) \right) \\ &= \det \left[ (\mathbf{F}_N \otimes \mathbf{I}_M) \Xi (\mathbf{F}_N^H \otimes \mathbf{I}_M) + (\mathbf{F}_N \otimes \mathbf{I}_M) \Omega (\mathbf{F}_N^H \otimes \mathbf{I}_M) \right] \\ &= \det \left[ (\mathbf{F}_N \otimes \mathbf{I}_M) (\Xi + \Omega) (\mathbf{F}_N^H \otimes \mathbf{I}_M) \right] \\ &= \det (\Xi + \Omega), \quad (30) \end{aligned}$$

where

$$\Omega = \frac{E_s}{N_0} \sum_{i=1}^{P-1} \sum_{\substack{i'=i+1, \\ l_{i'} \neq l_i}}^P \left( h_i^* h_{i'} \Lambda + h_i h_{i'}^* \Lambda^H \right). \quad (31)$$

Since  $l_{i'} \neq l_i < M$ ,  $\Pi^{l_{i'}-l_i}$  is a permutation matrix that will not be a identity array, i.e., all elements on its diagonal are zero. Moreover,  $\Delta^{-k_i}$  and  $\Delta^{k_{i'}}$  are diagonal matrices, so all diagonal elements of  $\Lambda$  are zero, and therefore all diagonal elements of  $\Omega$  are zero.

Since  $\mathbf{H}_{DD}^H \mathbf{H}_{DD}$  is a semi-positive definite matrix and  $\mathbf{I}_{MN}$  is a positive definite matrix,  $(\mathbf{I}_{MN} + \mathbf{H}_{DD}^H \mathbf{H}_{DD})$  is a positive definite matrix. Because  $(\Xi + \Omega)$  is a similarity matrix to  $(\mathbf{I}_{MN} + \mathbf{H}_{DD}^H \mathbf{H}_{DD})$ ,  $(\Xi + \Omega)$  is also a positive definite matrix. Moreover,  $\Xi$  is a diagonal matrix and all diagonal elements of  $\Omega$  are zero. Because the determinant of a semi-positive definite matrix is not greater than the product of its diagonal elements [19, Theorem 11], we have

$$\det (\Xi + \Omega) \leq \det (\Xi). \quad (32)$$

By combining (26), (30) and (32), we have finished the proof of *Proposition 2*.

#### REFERENCES

- [1] Y. Xiao, Q. Du, W. Cheng, and N. Lu, "Secure communication guarantees for diverse extended-reality applications: A unified statistical security model," *IEEE Journal of Selected Topics in Signal Processing*, vol. 17, no. 5, pp. 1007–1021, Sep. 2023.
- [2] Y. Zhang, W. Cheng, and W. Zhang, "Multiple access integrated adaptive finite blocklength for ultra-low delay in 6G wireless networks," *IEEE Transactions on Wireless Communications*, vol. 23, no. 3, pp. 1670–1683, Jul. 2024.
- [3] C. Xu, L. Xiang, J. An, C. Dong, S. Sugiura, R. G. Maunder, L.-L. Yang, and L. Hanzo, "OTFS-aided RIS-assisted SAGIN systems outperform their OFDM counterparts in doubly selective high-Doppler scenarios," *IEEE Internet of Things Journal*, vol. 10, no. 1, pp. 682–703, Jan. 2023.
- [4] R. Hadani, S. Rakib, M. Tsatsanis, A. Monk, A. J. Goldsmith, A. F. Molisch, and R. Calderbank, "Orthogonal time frequency space modulation," in *IEEE Wireless Communications and Networking Conference*, San Francisco, CA, Mar. 2017, pp. 1–6.
- [5] Z. Wei, W. Yuan, S. Li, J. Yuan, G. Bharatula, R. Hadani, and L. Hanzo, "Orthogonal time-frequency space modulation: A promising next-generation waveform," *IEEE Wireless Communications*, vol. 28, no. 4, pp. 136–144, Aug. 2021.
- [6] P. Raviteja, K. T. Phan, and Y. Hong, "Embedded pilot-aided channel estimation for OTFS in delay-Doppler channels," *IEEE Transactions on Vehicular Technology*, vol. 68, no. 5, pp. 4906–4917, May 2019.
- [7] P. Raviteja, K. T. Phan, Q. Jin, Y. Hong, and E. Viterbo, "Low-complexity iterative detection for orthogonal time frequency space modulation," in *IEEE Wireless Communications and Networking Conference*, Barcelona, Spain, Apr. 2018, pp. 1–6.
- [8] W. Lin, Y. Yan, L. Li, Z. Han, and T. Matsumoto, "Semantic-forward relaying: A novel framework toward 6G cooperative communications," *IEEE Communications Letters*, vol. 28, no. 3, pp. 518–522, Mar. 2024.
- [9] Z. Zhao, Q. Du, and H. Song, "Traffic load learning towards early detection of intrusion in industrial mMTC networks," *IEEE Transactions on Industrial Informatics*, vol. 19, no. 7, pp. 8441–8451, Jul. 2023.
- [10] Y. Fu, W. Cheng, W. Zhang, and J. Wang, "Scalable extraction based semantic communication for 6G wireless networks," *IEEE Communications Magazine*, vol. 62, no. 7, pp. 96–102, Jul. 2024.
- [11] W. Lin, Y. Yan, L. Li, Z. Han, and T. Matsumoto, "SemantIC: Semantic interference cancellation toward 6G wireless communications," *IEEE Communications Letters*, vol. 28, no. 8, pp. 1810–1814, Aug. 2024.
- [12] W. Lin, L. Li, J. Yuan, Z. Han, M. Juntti, and T. Matsumoto, "Cooperative lossy communications in unmanned aerial vehicle networks: Age-of-information with outage probability," *IEEE Transactions on Vehicular Technology*, vol. 70, no. 10, pp. 10 105–10 120, Oct. 2021.
- [13] T. Matsumoto, A. Zribi, R. Asvadi, E. Dupraz, and W. Lin, "Two-stage successive Wyner-Ziv lossy forward relaying for lossy communications: Rate-distortion and outage probability analyses," *IEEE Transactions on Vehicular Technology*, 2024, Early Access.
- [14] C. E. Shannon, "Coding theorems for a discrete source with a fidelity criterion," *IRE Nat. Conv. Rec.*, vol. 4, no. 1, pp. 142–163, Mar. 1959.
- [15] P. Raviteja, K. T. Phan, Y. Hong, and E. Viterbo, "Interference cancellation and iterative detection for orthogonal time frequency space modulation," *IEEE Transactions on Wireless Communications*, vol. 17, no. 10, pp. 6501–6515, Oct. 2018.
- [16] R. Chong, S. Li, W. Yuan, and J. Yuan, "Outage analysis for OTFS-based single user and multi-user transmissions," in *IEEE International Conference on Communications Workshops*, Seoul, Republic of Korea, May 2022, pp. 746–751.
- [17] S. M. Ross, *Introduction to Probability and Statistics for Engineers and Scientists*. Academic Press, 2000.
- [18] A. Barbu and S.-C. Zhu, *Monte Carlo Methods*. Singapore: Springer, 2020.
- [19] M. Rózański, R. Wituła, and E. Hetmaniok, "More subtle versions of the Hadamard inequality," *Linear Algebra and its Applications*, vol. 532, pp. 500–511, Nov. 2017.